JOURNAL OF AIRCRAFT
Vol. 46, No. 1, January–February 2009

Analysis and Design of a Flap-Equipped Low-Twist Rotor for Hover

A. Gagliardi*
Glasgow University, Glasgow, Scotland G12 8QQ, United Kingdom
and
G. N. Barakos†
Liverpool University, Liverpool, England L69_3GH, United Kingdom

DOI: 10.2514/1.34275

This study evaluates the potential benefits that fixed but deployable trailing-edge flaps may have on a low-twist hovering rotor using a blade-element method combined with two-dimensional and three-dimensional computational fluid dynamics. Low blade twist is beneficial in terms of forward-flight performance, which, combined with a deployable flap, could also offer good hover performance, resulting in an overall better design in comparison with a plain twisted blade. To evaluate this concept, a parametric study of flap configurations was conducted using a simple blade-element method based on computational-fluid-dynamics-generated two-dimensional aerodynamics. This simple model indicated that up to 6 deg of blade twist could be recovered at high rotor thrust by using an optimized flap configuration. Performance improvements were also obtained for outboard slotted-flap configurations. The optimum slotted-flap designs were also evaluated using three-dimensional computational fluid dynamics, which confirmed that an inboard flap combined with a low-twist (−7 deg) rotor blade matched the performance of a plain blade with −13 deg of twist. A blended-flap configuration was also applied and evaluated. This simpler design demonstrated the equivalent performance of a clean rotor with 10 deg of blade twist, providing further evidence of the potential of the fixed inboard flap concept.

Nomenclature

C_Q	=	torque coefficient, $Q/0.5\rho\pi R^3(\Omega R)^2$
C_T	=	thrust coefficient, $T/0.5\rho\pi R^2(\Omega R)^2$
C_p	=	pressure coefficient $(P_\infty - P)/\frac{1}{2}\rho U^2$ scaled along the blade by $1/R^2$
c	=	nondimensional blade chord
FM	=	figure of merit, $0.707(C_T^{1.5}/C_Q)$
k	=	turbulent kinetic energy
R	=	nondimensional blade radius
r	=	nondimensional blade span location
β_0	=	coning angle, deg
δ	=	flap deflection angle, deg
θ_0	=	collective pitch at $0.75R$, deg
λ_2	=	second eigenvalue of $\mathbf{S}^2 + \Omega^2$
ω	=	specific rate of dissipation

I. Introduction

IN THE design of main rotor blades, performances in hover and forward flight must be considered and balanced. This is mainly achieved by using simple blade-element methods or comprehensive rotor analysis tools combined with wind-tunnel testing and followed by flight tests. The latter two prove to be an expensive element in the design process and usually offer a narrow test matrix due to high costs. On the other hand, computational models have the ability to evaluate a variety of flight conditions by using 2-D aerodynamic data and theoretical flight mechanics [1–4]. Compared with both wind-tunnel and flight-testing, computer models offer a fast and cost-effective alternative. However, due to the complexity of the aerodynamic and aeroelastic problems encountered on a rotor blade, the accuracy of simple blade-element methods or even comprehensive codes is still considered to be insufficient, with experimental testing required for validation. Therefore, an evident gap exists in the design chain for an accurate method that will be able to verify model predictions and give a greater insight into the rotor flow environment. In turn, this could help reduce the amount of experimental testing required for validation and cut costs associated with model manufacturing and wind-tunnel time, thus promoting a compact cost-effective design process for future rotor blade development.

An appropriate candidate for this purpose would be computational fluid dynamics (CFD) based on high-fidelity Reynolds-averaged Navier–Stokes (RANS) solvers. Research using RANS has been proven to offer accurate aerodynamic loads predictions and detailed flowfield visualizations, with the list of publications being too long for reference here. Initially, CFD development for rotors was limited to inviscid Euler calculations [5]. However, due to the increased complexity of the rotor flow environment, including rotating-blade motion, blade–vortex and blade–wake interactions, localized blade stall, and vibratory loadings to name but a few, viscous calculations are necessary. Fortunately, technological advances in computing power and CFD algorithms make the daily use of RANS CFD in the design and development process more feasible and, as numerical algorithms have evolved, so has the accuracy with which rotor flows can be predicted.

The current design analysis concentrates on the implications of blade twist on helicopter rotor performance. The hover efficiency of a rotor is judged in terms of the figure of merit (FM), which is the ratio of ideal power over actual power:

$$\mathrm{FM} = \frac{\text{ideal power}}{\text{actual power}} = \frac{C_T^{1.5}/\sqrt{2}}{C_Q} \tag{1}$$

The ideal power assumes that all thrust is produced with no power requirements. The actual power takes into account additional effects that contribute to increased rotor power, such as pressure drag and induced drag. The higher the FM, the better the hovering efficiency

Received 4 November 2007; revision received 22 April 2008; accepted for publication 26 April 2008.

*Ph.D. Candidate, Department of Aerospace Engineering; a.gagliardi@aero.gla.ac.uk.
†Reader, Computational Fluid Dynamics Laboratory, Department of Engineering; G.Barakos@Liverpool.ac.uk (Corresponding Author).

of a rotor. The main detrimental factor in a helicopter's hovering performance is heavy loading at the blade tip associated with increased strength of the tip vortices and high induced drag. There are several passive methods that can improve hover efficiency. Blade taper, swept tips, and varying tip angles can all have beneficial effects. For example, a recent design study by Le Pape and Beaumier [6] used CFD to optimize a rotor for hover using such design constraints. The final design included a parabolic swept tip with a large anhedral deflection angle. However, the most common method is to implement twist along the span of the rotor in an attempt to redistribute the loading on the blade more evenly. This results in a rotor with lower tip loading, which can achieve good performance by means of reducing induced power effects due to a weaker tip vortex.

In blade design, a compromise normally has to be reached between hover and forward-flight performances. For large helicopters that require long periods of hovering, highly twisted blades help to ensure optimum efficiency. On the other hand, light 2- or 3-bladed helicopters generally have very low levels of blade twist, because they will operate in forward flight more than in hover. In steady level flight, the advancing blade may produce large amounts of lift and can approach near-sonic speeds at the blade tip. However, it is beneficial for limiting induced power and noise if the strength of shocks is kept to a minimum; consequently, designers will target a local angle of attack at the blade tip around the zero-lift angle. Unfortunately, large amounts of blade twist can make this very difficult to achieve, due to the increase in inboard loading, the consequence of which is a negative effective angle at the blade tip and the formation of shocks on the lower blade surface. Shock formation reduces thrust, increases control loads, and reduces the working life of rotor blades. Keys et al. [7] provide several plots to quantify the aforementioned effects.

In view of the preceding, being able to achieve good hover performance with as little blade twist as possible would seem ideal. This was investigated by Noonan et al. [8] with the HIMARCS I (High Maneuverability and Agility Rotor and Control System) model rotor. Details of the blade geometry for the HIMARCS I can be found in Table 1. The high-lift devices tested included a 3 deg slotted-flap and two leading-edge slat designs near the blade tip. These would be deployed in hover and retracted for forward flight. Some benefits were evident with the −6 deg leading-edge slat design, but the results for the slotted flap were inconclusive [8]. Therefore, it is still to be seen whether there is a future in this concept. The idea of using fixed flaps was given further consideration in experiments and computations by Wachspress and Quackenbush [9]. They demonstrated that fixed inboard flaps were capable of reducing blade–vortex interaction (BVI) noise in low-speed axial descent. By deploying inboard flaps, they noted an inboard shift in circulation and greater wake mixing due to the flap edge vortex (FEV) diluting the tip vortex. The most recent research into the use of flapped rotors in hover was published by the authors [10,11]. Based on [8], the concept of twist recovery using inboard and outboard fixed flaps on a low-twist blade was investigated using a combination of blade-element methods and CFD. A limited number of flap locations, spanwise lengths, and deflection angles were considered, suggesting that up to 6 deg of blade twist could be recovered by means of an inboard flap at high thrust.

To date, the majority of flapped-rotor research has looked at obtaining a *jet-smooth ride* for rotorcraft by attempting to reduce hub vibrations and BVI noise. No 3-D viscous CFD on flapped rotors has to date been published in either hover or forward flight. These problems require large grids, substantial computational power, and special mesh treatment such as overset grids [12] to fully capture the physics of the flow. Full-scale rotor experiments have also concentrated on vibration and BVI noise reduction. Therefore, the aim of this research is to consider the application of trailing-edge flaps on low-twist rotors for hover performance improvement. This is achieved by the following steps:

1) Combine a simple aeromechanical model for rotorcraft analysis with 2-D CFD to evaluate the flapped-rotor concept.

2) Verify the results of step 1 by evaluating the optimum designs using 3-D Euler and RANS hover calculations.

3) Compare the performance of plain flaps with flaps blended with the main element (without tips) because this design may be more likely to reach application.

As far as the authors are aware, this is the first comprehensive computational study using CFD to analyze flapped-rotor performance in hover.

Table 1 HIMARCS I [8] rotor data

Span	Twist	Section detail
0–12.2%R	1 to 0 deg	Shaft axis to root cutout
12.2–22.4%R	0 to −1 deg	Root cutout to RC(4)-10
22.4–80%R	−1 to −5.4 deg	RC(4)-10
80–85%R	−5.4 to −5.8 deg	Transition
85–100%R	−5.8 to −7°	RC(6)-08, high-lift devices
Rotor radius R	56.224 in.	Blade chord c, 4.454 in.
Rotor solidity	0.101	M_T 0.627

II. Computational Tools

The methods used for all computations in this research are now briefly described.

A. Blade-Element Methods

The low-order model used in this research is based on the blade-element method [13]. It allows for the simplification of the 3-D rotor problem by relying on 2-D sectional aerodynamic lookup tables to reduce computational times. Time dependency via indicial methods [14] and 3-D wake effects can introduce further accuracy by accounting for boundary-layer lag and tip-vortex convection. Finally, modeling of the separated flow can be introduced by implementing models such as the Leishman–Beddoes dynamic stall model [15].

The blade-element method described herein is used for the calculation of rotor loads while in hover. Hover, for reasons of simplicity, can be considered to be a steady-state problem in which the inflow velocity at each specific location along a blade remains constant in time. The present method allows for spanwise and chordwise variation of loading. The blade is discretized into a number of 1-D sections along the span. Each 1-D section requires geometric and aerodynamic data to be supplied. Aerodynamic data are provided at Mach numbers ranging from 0.3 to 0.9 and include sectional zero-lift angle, stall angle, lift-curve slope, as well as pre- and poststall behavior, with a total of 19 parameters required. The necessary geometric data include information regarding the radial variation of chord, twist, and sweep. For each time step, the local loading is calculated at each radial element for a given azimuth, followed by integration and progressive stepping through the azimuth range. A prescribed wake method is implemented to model the downwash. The model has been previously validated by Beedy et al. [16].

B. Helicopter Multi-Block Solver

All CFD computations were performed using the Helicopter Multi-Block (HMB) flow solver [17]. The solver has been successfully applied to a variety of problems, including rotorcraft in hover and forward flight [18], dynamic stall [19], and BVI [20]. HMB solves the unsteady RANS (URANS) equations on multiblock-structured grids in serial or parallel mode using a cell-centered finite volume method. The convective terms are discretized using either Osher and Chakravarthy's [21] or Roe's [22] scheme. MUSCL interpolation is used to provide formally third-order accuracy, and the Van Albada limiter is used to avoid spurious oscillations across shocks. The time-marching of the solution is based on an implicit dual-time-stepping method. The final algebraic system of equations is solved using a conjugate gradient method in conjunction with block incomplete lower/upper factorization. Several one- and two-equation turbulence models are available. For the present work, all CFD calculations are performed using the standard k-ω model of Wilcox [23]. Extensive validation for

hovering rotors has also been performed [18]. For hovering rotors, two types of far-field boundary conditions are used. The first is based on imposing freestream/linear extrapolation at the far field of the computational domain. The second approach is a potential sink (or Froude) boundary condition and is designed to suppress flow recirculation near the outflow boundary. A potential sink is placed at the rotor origin and, based on actuator-disk theory, a constant axial (outflow) velocity is prescribed on a circular part of the outflow boundary face. The size of the outflow area is determined by

$$\frac{R_{\text{outflow}}}{R} = 0.78 + 0.22e^{-d_{\text{outflow}}/R} \tag{2}$$

where R is the rotor span, R_{outflow} is the outflow radius of the wake, and d_{outflow} is the distance of the rotor to the outflow boundary. The strength of the sink is chosen to balance the mass flow in and out of the computational domain.

III. Design Methodology: Blade-Element Method

The analysis of flapped rotors in hover requires the rapid assessment of many flap configurations and comparisons with clean blades over a wide range of thrust settings. The CPU demands of 3-D CFD is too expensive to conduct such a venture alone. These demands include the time required to generate the necessary surface boundaries and to produce high-quality block-structured grids, However, simpler models such as the blade-element method used in the current work lend themselves well to such studies.

Although simple models lack the fidelity offered by CFD, with the provision of 2-D aerodynamics, these models allow for a time-efficient analysis of various flight conditions. Table 2 highlights the various CPU times required by the methods used in this study for calculating the performance of a rotor in hover. The blade-element method is capable of evaluating over 7000 design conditions in under 3 h on a single 2.4 GHz Pentium 4 processor with 1 GB RAM. Calculations to obtain 2-D aerodynamic data (at a single Mach number and for a single blade section) for input into the model can take up to 8 h alone. Although both methods are more time-efficient than 3-D CFD, single hover computations, based on the Navier–Stokes equations, offer much more detail in both blade loadings and flowfield visualizations.

Blade-element computations were performed for a range of flap configurations over a range of thrust and trim settings. The flap parameters selected for investigation were 1) flap deflection angle, 2) flap location, 3) flap chordwise length, and 4) flap spanwise length. The employed blade-element method splits the blade boundary into 44 sections and, with the exception of the most inboard element, the whole length of the blade was considered in the design process. Certain constraints had to be applied on the possible flap configurations for the design to be viable. First, the maximum length of the flap had to be restricted due to potential problems with blade elasticity. The blade chord was limited in size to that used in the original experiment, because a flap too large could lead to structural problems. The original work in the HIMARCS I experiment considered a clean rotor and one with a slotted flap with a fixed chord and deflection angle at the blade tip. To take into account variations in flap chord, slotted-flap configurations, geometrically equivalent to the designs employed in HIMARCS I were considered. Flap-chord sizing was accomplished by extracting the geometric data of the original design and scaling by a factor of 33 and 66% of the original flap geometry. The new geometry was then superpositioned on clean sections with an approximation to the slot geometry accounted for in the same way. To reduce the number of 2-D URANS calculations, flap-chord lengths of 22 and 11%c were considered by running CFD calculations at $M = 0.5$ and $Re = 3 \times 10^6$, which is the middle region of the test matrix used for the rest of the 2-D calculations. A ratio of the extracted coefficients between the original 32%c slotted flap and the new results was then implemented. Variations in flap deflection angle could not be treated in the same way due to the need to properly model the influence of adverse pressure gradients at high flap deflection angles and boundary-layer mixing. Because no specification for the pivot point for the flap was given in the original report by Noonan et al. [8], this was estimated at $c/4$.

Each configuration is considered at various thrust coefficients from $C_T = 0.0005$ to 0.00829. At each thrust setting, the blade-element method uses a trimmer based on the Newton–Raphson scheme and approximates the trim settings based on an estimated helicopter weight. The rotor thrust is then recalculated via the updated trim settings, and the process continues until convergence to the designated thrust coefficient is achieved. In the model, the tolerance that the trimmer must match is on the order of 1%, which can be deemed satisfactory for what is already an approximate method. The model requires 8 retrimming steps to converge to a solution, which equates to a few seconds in real time.

Table 2 Grid size and CPU requirements for various methods

Method	Grid points	No. of CPUs [a]	Designs	Clock time, h
BEM	-	1	≈7700	≈2.5
2-D URANS CFD	85,000	1	40	≈8
3-D inviscid CFD	2.2×10^6	8	1	≈22
3-D viscous CFD	2.7×10^6	8	1	≈36
3-D viscous CFD	5.25×10^6	24	1	≈24

[a]2.4–3 Ghz P4 with 1 GB RAM.

IV. Grid Generation

The blocking scheme implemented for grid generation varies with respect to the blade design being considered. Individual blockings were required for clean and twisted blades, slotted-flap blades, and blended-flap blades. Each grid prepared in the current work was manually projected to the blade design considered and altered to define different blade collective and coning angles. Because periodic boundaries were applied for CFD and the HIMARCS I rotor [8] consisted of 4 blades, one-quarter of the rotor was modeled. The far-field boundaries were placed to roughly match the location of the wind-tunnel walls. All grids were prepared using the ICEMCFD-Hexa grid-generation software.

The blocking schemes implemented for clean and twisted blades were identical to each other. These consisted of H-H grids with an embedded C-grid around the rotor blade to obtain optimum mesh quality at the leading edge. The blade was treated as rectangular and the topology employed at the tip was similar to the one used in [19]. The root cutout was not modeled. The advantage of the employed multiblock topology is that it allows for flat and rounded tips and it can be modified to account for the presence of integrated and slotted flaps. Details of the grids can be found in Table 3. The blocking scheme employed for the slotted-flap geometry was much more complex and was essentially a C-grid within a C-grid within the overall H-H topology. To allow for the inclusion of a multiblock topology around the flap, flap gaps of 1%R were included on either side of the flap.

Finally, rotor blades with blended trailing-edge flaps were considered. The blended flap is considered to have no flap gaps and, most important, the flap edges are closed and blended with the main blade geometry. Although formally based on the original clean-blade topology, an increase in the number of blocks was required to account for the blended region between the blade and the flap. To ensure that the results were grid-independent, the mesh density (particularly in the region around the blade) was increased to levels concluded from a grid-dependency study. In total, 144 blocks were required to model the inviscid blade, with 178 blocks required for the viscous blade. The increase in blocks for viscous calculations follows a greater requirement for even point distribution at the blending region on the blade.

V. Validation Results

A grid-dependency study was first conducted for the baseline HIMARCS I rotor. Grid sizes of approximately 1.5, 2.65, and

Table 3 Details for 3-D inviscid and viscous grids

Geometry	Blocks	First cell size (main:tips)	Surface grid points (blade:flap:total)
		Inviscid	
Clean blade	106	$10^{-4}c$:$10^{-4}c$	16,000:0:2.2×10^6
Optimized flaps	446	$10^{-3}c$:$10^{-3}c$	22,000:1500:2.6×10^6
Clean blade with blended flap T	144	$10^{-4}c$:$10^{-4}c$	48,000:06.5×10^6
	144	$10^{-4}c$:$10^{-4}c$	35,000:13,000:6.5×10^6
		Viscous	
Clean blade	106	$10^{-5}c$:$10^{-4}c$	18,000:0:2.7×10^6
Clean blade with blended flap T	178	$10^{-5}c$:$10^{-4}c$	48,000:0:5.3×10^6
	178	$10^{-5}c$:$10^{-4}c$	35,000:13,000:5.3×10^6

4.8 million points were compared for viscous solutions in hover. Convergence to a C_T of 0.00829 was achieved for all three grids and the respective results for C_Q and FM were evaluated. Grid convergence required about 5 million points. Next, the effect of wake resolution on the computed blade loads was evaluated. This involved taking a fine grid that would provide grid-independent solutions and reducing the number of points normal or around the blade and in its wake by 10 and 20%. Starting from a grid of 5.25 million points, the reduced wake resolution has had the effect of reducing the average blade loads by less than 1% in the most extreme case.

Finally, validation against the HIMARCS I model rotor's tunnel data is offered in Fig. 1. Before the results are discussed, a few factors should be considered with respect to the experiment itself. First, the experiment employed a model fuselage with a hub during testing, whereas the current work assumes an isolated rotor with a modeled shaft. Second, the rotor trim settings of the experiment were not known. To overcome this, the blade-element method was employed to estimate the rotor trim, which was then built in to the rotor blade geometry. Third, the published data for validation were just C_T, C_Q, and FM, and predictions for these are subject to high error margins (± 0.07).

Figures 1a and 1b compare C_Q versus C_T and C_T versus FM for the medium, inviscid, and viscous grids used in the current work. The inviscid CFD gives reasonable predictions compared with the experiment, but overpredicts at medium-to-high thrust settings, which is to be expected because these calculations do not account for drag and blade stall. The viscous CFD results compare better with experiments and capture their trend adequately. The slight dip in performance for the viscous solution could be attributed to the turbulence model underpredicting blade stall, a well-known issue regarding the k-ω model in aerospace applications [24,25]. For results obtained using the finer grids (see Figs. 1c and 1d), two separate boundary conditions were applied to further investigate this issue. The first set of results used the original far-field domains as in the experiment, with the second set of results having the far field and outflow located at 4 times the blade span. The results using the experimental boundaries demonstrate the dip in performance at high thrusts as with the previous results. Extending the far-field boundaries, however, improves predictions and eliminates the element of blade stall. Investigation of the flowfield indicated that the loss in performance evident with the narrow domain is due to the tip vortex striking the proceeding blade because of strong upwash caused by the far-field wall being too close, with the blade–vortex interaction causing local blade stall at high C_T values. Extending the domain reduces the strength of the upwash and the vortex passes beneath the blade, as expected. It is interesting to note, though, that both sets of results fall within experimental errors. Nonetheless, in the current study, we are interested only in the relative differences in predictions between various configurations, with satisfactory validation of the solver achieved for all test cases. Further validation of HMB can be found in [18]. Finally, the geometric data supplied for the RC(4)-10 and RC(6)-08 blade sections gave a poor description of the leading edge of the rotor blade, which may have had an influence on results.

VI. Parametric Study and Optimum Design

The parametric study of the various flap configurations considered for analysis follows. Details of the parameter space for the study can be found in Table 4, with flap sizes and locations given as a percentage of blade span, $\%R$. For each flap location, the flap span, chord, and deflection angles were varied, which resulted in the evaluation of over 396 designs for the inboard and 120 designs for the outboard configurations. This was repeated for a range of C_T between 0.0005 and 0.00829. All calculations were performed at a rotor tip Mach number of 0.627.

Results show that when the flap defection angle is increased from 3 to 10 deg, the inboard flap gives a large performance increase of 4.7% over the baseline rotor, which is equivalent to a rotor with -13 deg of twist. The best an outboard flap can offer is a reduction in performance of 2% at a high thrust setting, which agrees well with the trend for the original slotted-flap design tested in the HIMARCS I experiment [8].

A summary of the optimum designs and the potential performance enhancement that they offer is presented in Tables 5 and 6 for the inboard and outboard flaps, respectively. Based on these tables, the optimum designs for both inboard and outboard flaps were selected to be verified using 3-D CFD. From Table 5, the inboard flap gives a performance increase at very low thrust settings of 6%, with very little effect at medium thrust, and consistent improvements of more than 4% at high thrust. At lower thrust, the smallest flap chord and deflection angle gives the best performance. This is also true of the flap spanwise length with the flap location being closer to the blade root. At the higher thrust coefficients, the optimum flap span, chord, and deflection angle are consistent at $24\%R$, $32\%c$, and 10 deg, respectively, with the optimum flap location shifting outboard as the blade loading increases. Table 6 lists the optimum outboard flap configurations at various C_T. As with the inboard flap at low thrust, the smallest flap chord and deflection angle offer the optimum performance, although in this case, it does not always offer an improvement. At medium thrust, the optimum configuration varies, but performance improvements of up to 9% are possible. Finally, at high thrust settings, the outboard flap gives no improvements in performance.

Based on these results, there are three or four designs that could be implemented. Therefore, a decision was made to select a flap design that was located sufficiently inboard (i.e., avoided the blade root and allowed for a closed blade tip), unlike the original HIMARCS I flapped rotor. A schematic of the optimum configuration and expected performance can be found in Fig. 2. The flaps selected were the 1) inboard flap location of $36\%R$, flap span of $24\%R$, flap chord of $32\%c$, and flap deflection angle of 10 deg and 2) outboard flap location of $92\%R$, flap span of $8\%R$, flap chord of $32\%c$, and flap deflection angle of 10 deg. The optimum inboard flap configuration should offer performance improvements of between 3–4% at high thrust settings. The optimum outboard flap should offer improvements of up to 9%.

VII. Results for the Optimum Blade Design

A. Clean Blades of Varying Twist

Inviscid and viscous grids for blades with linear twists of -4 and -13 deg were considered to evaluate this effect. Inviscid

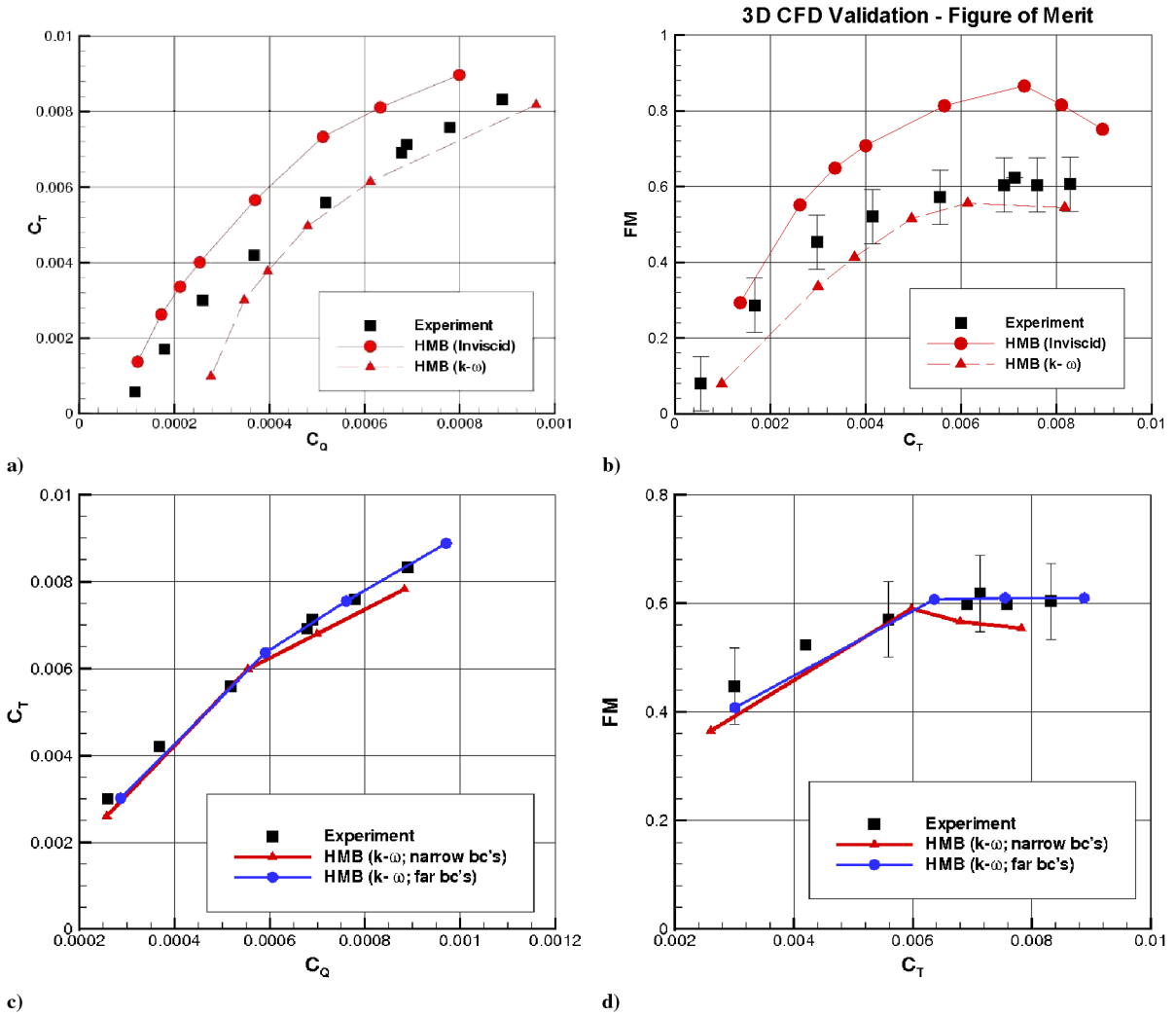

Fig. 1 HIMARCS I hover performance validation: a) blocking A: C_T vs C_Q, b) blocking A: FM vs C_T, c) blocking B: C_T vs C_Q, and d) blocking B: FM vs C_T; $Re = 168,000$ and k-ω turbulence model; bc denotes boundary conditions.

Table 4 Summary of the parameter space investigated in the parametric study

Parametric study test matrix.					
	Flap location	Flap span	Flap chord	Flap angle	Designs
Inboard	28–68%R	4–24%R	32, 22.33, and 11.67%c	3 and 10 deg	396 at 15 C_T
Outboard	90–96%R	2–10%R	32, 22.33, and 11.67%c	3 and 10 deg	120 at 15 C_T

Table 5 Optimum inboard flap designs at various C_T; bold indicates the optimum design

		Inboard flap optimization				
C_T	FM	Flap size, %R	Flap location, %R	Flap deflection, deg	Flap chord, %R	Change in percent, %
0.000545455	0.2128	24	68	3	10.67	6.5
0.0007	0.2958	24	68	3	10.67	5.8
0.0012	0.5495	4	32	3	10.67	1.3
0.0015942	0.7035	8	28	3	10.67	0.12
0.00167273	0.7262	4	28	3	10.67	0
0.0019	0.7793	4	28	3	10.67	0.26
0.0022	0.8348	4	28	10	10.67	0.8
0.0025	0.8672	19.6	28	10	21.33	0.69
0.0028	0.8890	19.6	28	10	32	2.1
0.00298182	0.8889	24	28	10	32	2.3
0.00414545	**0.8674**	**24**	**36**	**10**	**32**	**4.3**
0.00556364	0.8305	24	40	10	32	4.6
0.00690909	0.8017	24	44	10	32	4.7
0.00712727	0.7968	24	48	10	32	4.6
0.00829091	0.7770	24	48	10	32	4.7

Table 6 Optimum outboard flap designs at various C_T; bold indicates the optimum design

		Outboard flap optimization				
C_T	FM	Flap size, %R	Flap location, %R	Flap deflection, deg	Flap chord, %R	Change in percent, %
0.000545455	0.2011	2	90	3	10.67	0.65
0.0007	0.2618	8	90	3	10.67	−6.4
0.0012	0.5290	4	90	3	10.67	−2.45
0.0015942	0.7099	6	90	3	10.67	1
0.00167273	0.7367	8	92	3	10.67	1.4
0.0019	0.8042	4	94	3	10.67	3.5
0.0022	0.8743	6	94	3	10.67	5.6
0.0025	0.9224	10	92	10	10.67	7.1
0.0028	0.9458	10	92	10	32	8.7
0.00298182	**0.9481**	**8**	**92**	**10**	**32**	**9**
0.00414545	0.8582	6	94	10	32	3.2
0.00556364	0.7708	2	90	3	10.67	−3
0.00690909	0.7450	8	90	3	32	−2.7
0.00712727	0.7512	2	90	3	21.33	−1.4
0.00829091	0.7276	2	90	3	32	−1.9

computations for a range of thrust settings between 0.002 and 0.01 were run and the obtained results were compared against the HIMARCS I blade with −7 deg of twist [8] in Figs. 3a and 3b. As is evident, the highly twisted blade has an advantage at moderate-to-high thrust settings. At lower thrust values, the differences between the −7 and −13 deg blades diminish. To further establish this conclusion, viscous computations were performed for the highly twisted blade at high thrust settings (see Figs. 3a and 3b). The viscous computations indicate the same conclusions as the inviscid hover calculations regarding the effect of twist.

The results obtained so far have established confidence in the CFD method and helped to quantify the effect of blade twist in improving hover performance. In addition, the obtained results set a standard for the expected performance of the flapped rotor. Results from the parametric study predicted that the flapped blade with just −7 deg of twist should meet or exceed the performance of the highly twisted (−13 deg) rotor.

B. Hovering Rotors with Slotted Flaps

Next, the optimum inboard and outboard flap configurations suggested by the blade-element analysis were assessed using CFD (see Table 3). Because of the complexity of the employed multiblock topology, the requirements to model the near-flap region, as well as to resolve the flap loading, an increase in the number of points was necessary, in comparison with the clean blade. CFD results, including the trim states, were obtained for the optimum blade designs for a whole range of thrust settings. These are plotted in Figs. 4a–4d, along with the results for the clean rotors with −7 and −13 deg of twist.

Confirming the predictions of the blade-element method, the optimum inboard flap is shown to match and exceed the performance of the highly twisted blade for high thrust settings, as can be seen in Figs. 4a and 4c. Another encouraging result from Figs. 4b and 4d is that the optimum inboard flap design equaled the performance of the −13 deg twisted blade, but with reduced collective and coning angles

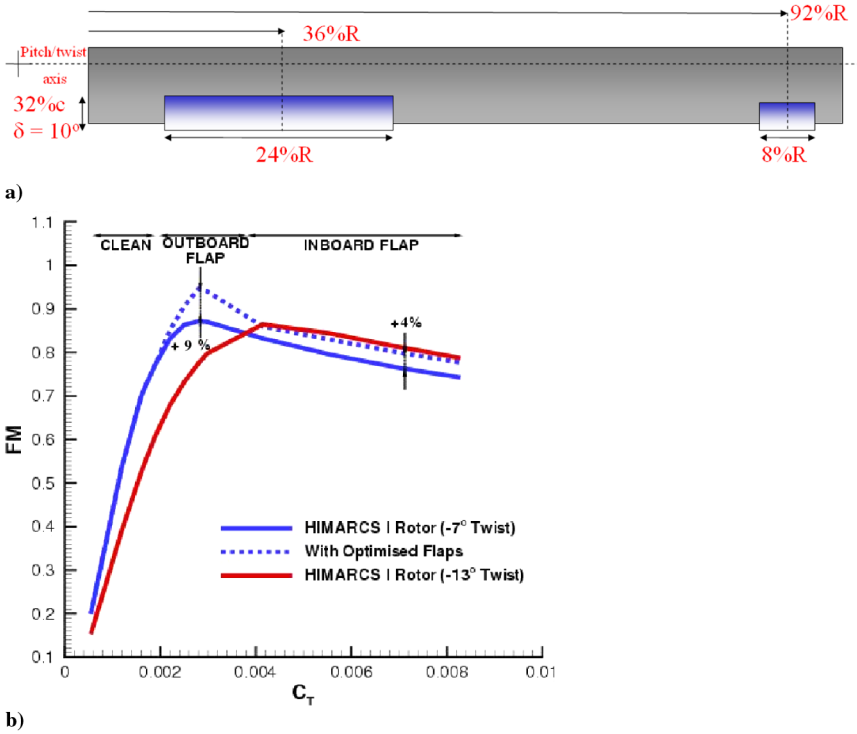

Fig. 2 Results for optimum design for the range of thrust coefficients: a) deployment schedule for fixed flap in hover and b) schematic of HIMARCS I with optimized flaps.

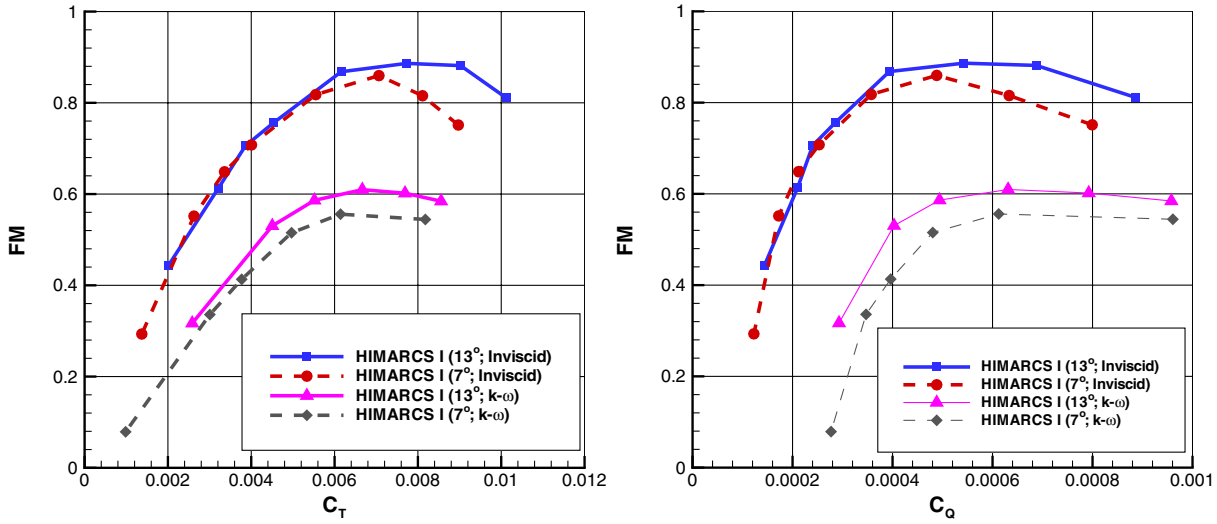

a) b)

Fig. 3 Three-dimensional CFD results showing the effect of blade twist: a) C_T vs FM and b) C_Q vs FM.

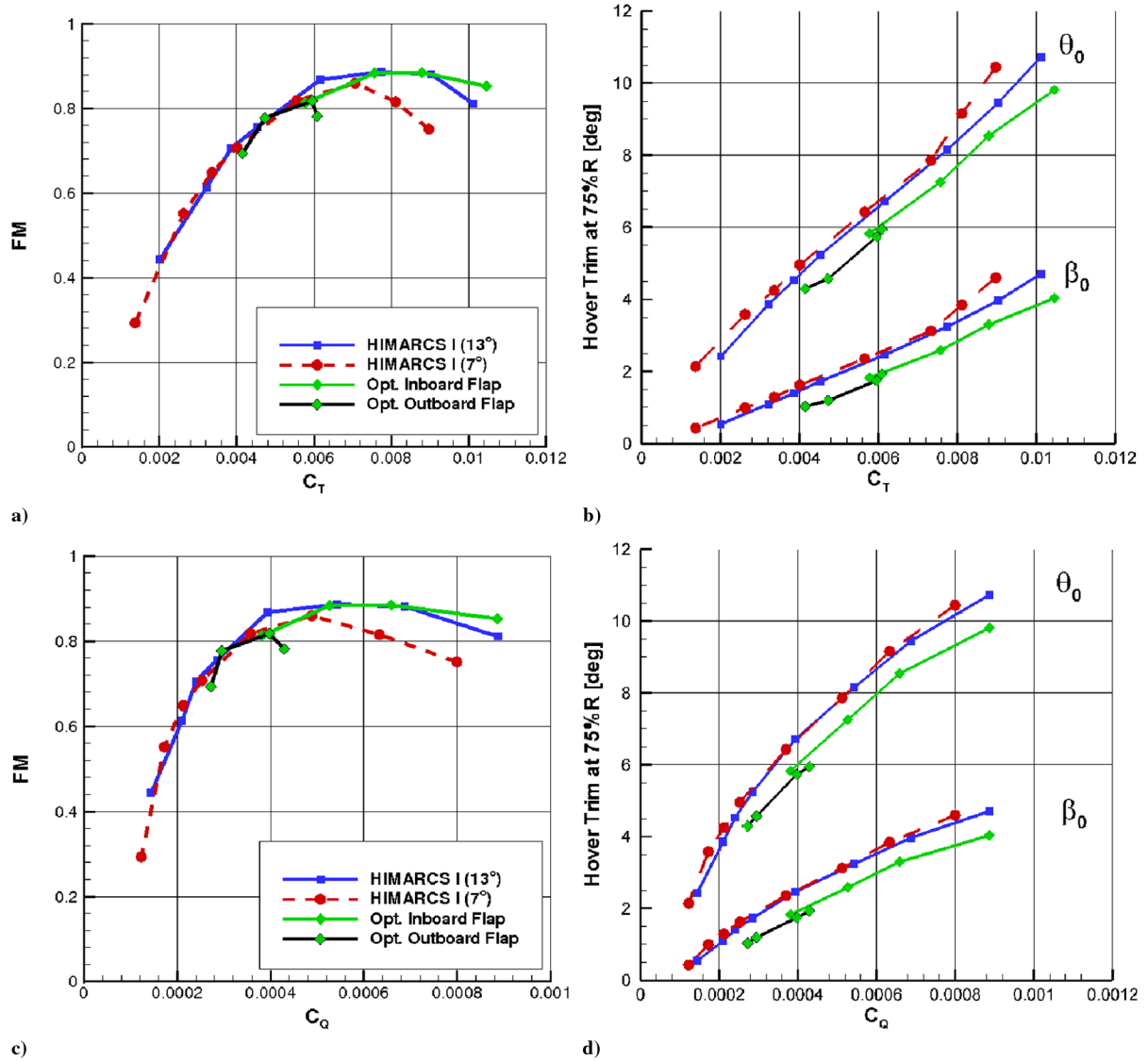

a) b)

c) d)

Fig. 4 CFD results for optimized flaps: a) C_T vs FM, b) C_T vs trim, c) C_Q vs FM, and d) C_Q vs trim.

of between 0.5–1 deg. The CFD results for the outboard flap configuration indicate poor performance compared with blade-element predictions. However, it does demonstrate the same range of thrust coefficients for best performance, as well as similar savings in blade trim angles as with the inboard flap (see Figs. 4b and 4d).

C. Hover Trim Settings

So far, all trim settings used to setup the rotor geometry in hover were calculated using the blade-element method, as described in the previous chapter. However, it would be beneficial if we could compare the accuracy of the blade-element method (BEM) with a high-fidelity method such as 3-D RANS CFD. The CFD solver has a built-in trim routine, which is similar to that used in the simple BEM. Unlike the 3-D RANS method, for which the predictive nature extends to the pressure on the surfaces and in the fluid around it, the BEM is entirely dependent on the input of external aerodynamic tables or polynomials, which is supplied by 2-D CFD-generated aerodynamic lookup tables in this case.

Figure 5 presents the predicted C_T versus FM and trim settings for the HIMARCS I rotors with −7 and −13 deg of twist. The graphs include viscous CFD results predicted from geometries set up using trim settings obtained from the BEM and inviscid CFD hover trimmer. There was little difference in the predicted performance between the BEM and the inviscid trimmer. However, in general, the CFD trim settings have predicted better performance than the trim settings predicted by the BEM, which is shown in Figs. 5a and 5c. If one examines the actual trim settings themselves, the predicted collective angles θ_0 between the CFD and BEM for each C_T is slightly greater by approximately 0.2 and 0.6 deg for the low-twist and high-twist rotors, respectively. For the predicted coning angles β_0, we see similar differences of 0.8 and 1.7 deg for the low-twist and high-twist rotors, respectively. As expected, increasing the blade collective angle requires a higher coning angle for the rotor to produce the same amount of thrust. It is clear that better performance is predicted with a low θ_0–β_0 combination, as predicted by the CFD trimmer. However, these CFD trimmer calculations are computationally expensive, whereas the BEM trimmer offers turnover times that are 4–5 orders of magnitude faster with near similar accuracy.

D. Blended-Flap Rotors

If the flapped-rotor concept is to be considered for the purposes of hover, blended or integrated flaps could be adopted. With the advent of piezoceramic actuators [26,27] and the work being conducted by NASA on the active twist rotor [28,29] (ATR), the blended flap seems more feasible for application to a full-scale rotor. Because of the nature of the ATR having numerous actuators embedded along the blade, the failure of a single actuator would account for only a small proportion of the blade area, thus reducing lift imbalance due to failures. Moreover, the blade could be returned to its clean state much faster than with a hydraulic or pulley-based system (as used on the Kaman aircraft [30]), due to the nature of the piezoceramic bender design.

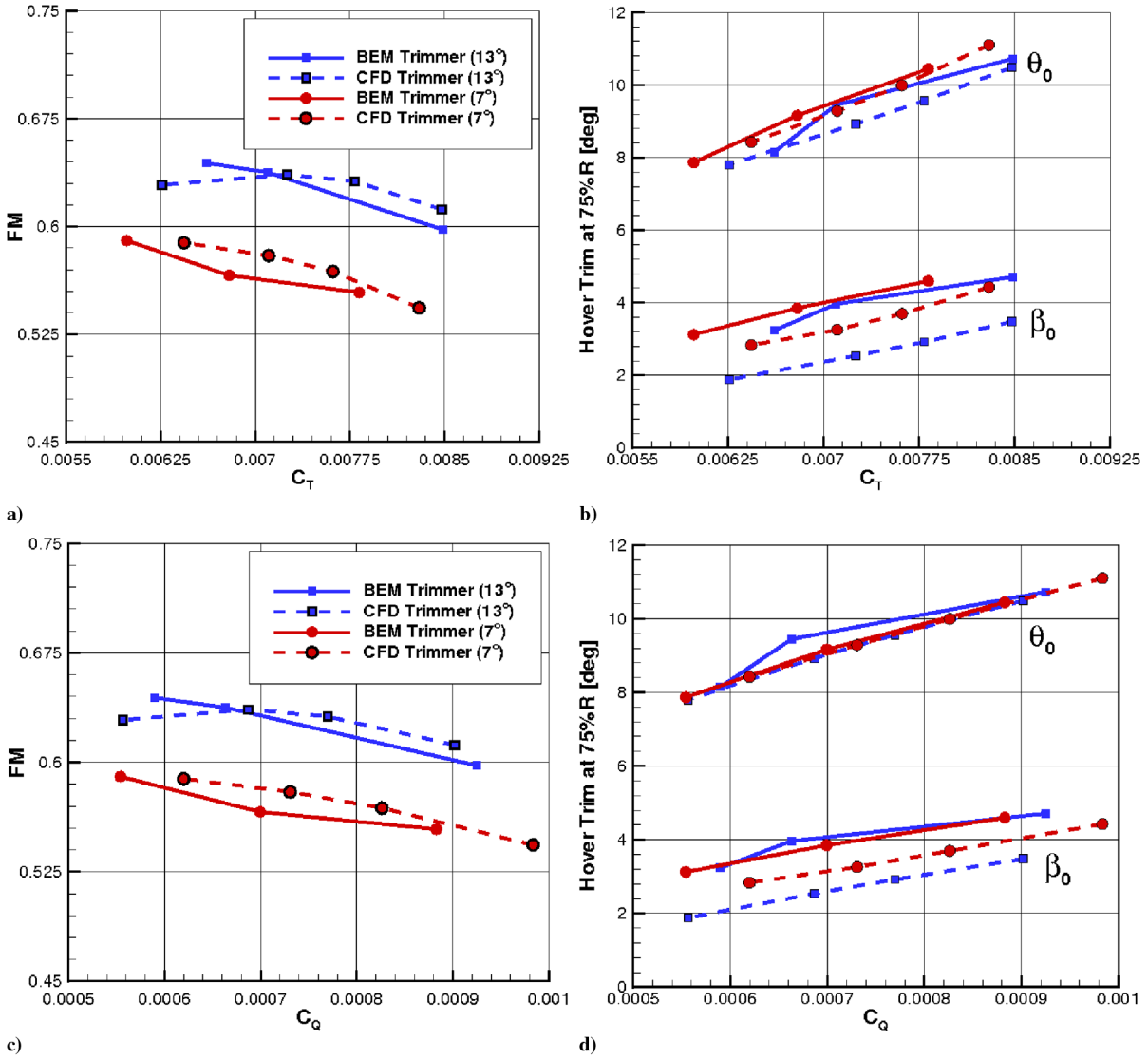

Fig. 5 Comparisons of 3-D CFD using predicted trim settings from BEM and inviscid CFD: a) C_T vs FM, b) C_T vs trim, c) C_Q vs FM, and d) C_Q vs trim.

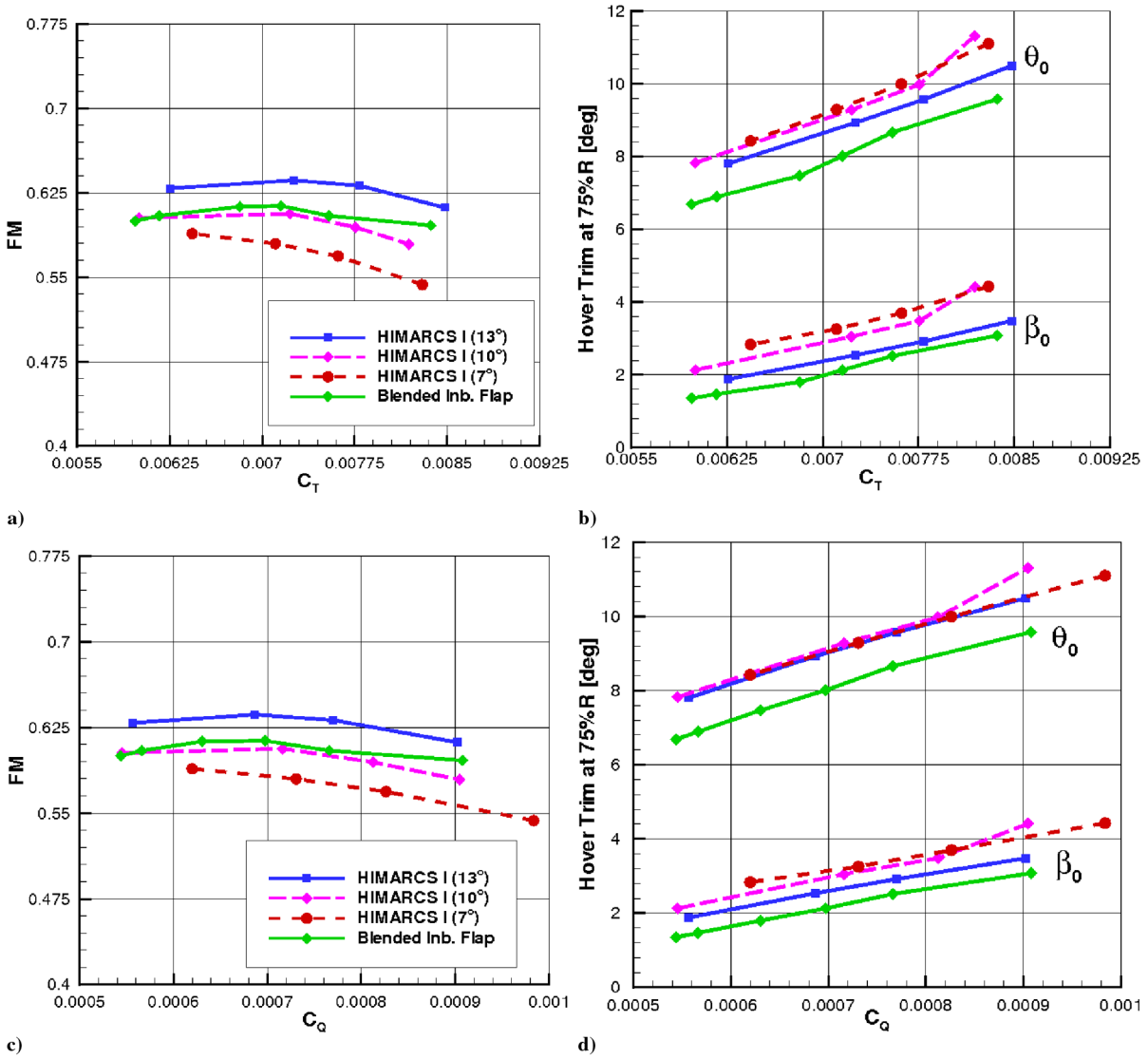

Fig. 6 Viscous 3-D CFD results for the HIMARCS I with −7, −10, and −13 deg of twist and blended inboard flap: a) C_T vs FM, b) C_T vs trim, c) C_Q vs FM, and d) C_Q vs trim.

The concept of a blended-flap rotor is thus considered. The optimum slotted inboard flap configuration was selected due to its success in the previous computations, compared with the outboard optimum design. The inboard flap would also undergo lower forces than with any outboard design, hence reducing power requirements for deployment and sustaining a fixed angle of deflection. The blended inboard flap was thus modeled by retaining the same flap spanwise length, chord length, and deflection angle as the optimum slotted-flap design. Calculations were first run using the inviscid CFD trimmer. The predicted trim settings from the CFD were then hard-wired into the rotor geometry and the flow then computed using viscous 3-D hover CFD.

The viscous results are presented in Fig. 6. The highly twisted rotors again show, as in Fig. 1, that increasing blade twist improves hover performance at high thrust coefficients. The low-twist rotor with 7 deg of twist and blended flap improves performance by up to 6.5%, which is comparable to a rotor with −10 deg of twist. Although an improvement of 6 deg was previously predicted by the slotted inboard flap, the reduced performance gains can be attributed to the lack of flap gap, which can improve C_l and delay separation on the flap. However, the flapped rotor also achieved increased performance with trim settings approximately 1 deg less than the baseline rotor.

Figure 7 presents isosurfaces of λ_2 colored by the turbulent Reynolds number for the HIMARCS I rotor with 10 deg of twist and the HIMARCS I rotor with blended inboard flap and 7 deg of twist, respectively. In Fig. 7a, we can see the shedding of the tip vortex, the root vortex, and a thin layer of vorticity leaving the trailing edge of the rotor. The higher levels of turbulence at the tip compared with the inboard region are highlighted by the levels of Re_T. The root vortex is seen to pass below the blade and is captured for a half-revolution. Further revolutions could be captured with higher values of λ_2, but are accompanied by a lack in clarity of solution as smaller elements of low pressure in the domain are captured. Further outboard, we can see the levels of turbulence change around the tip vortex as it rotates and passes into the wake, the higher values indicating the passage of the shed vortex itself. In Fig. 7b, we have the blended inboard flap configuration. Here, we have visualized the tip vortex, the spanwise sheet of vorticity from the blade's trailing edge, the flap edge vortices, and the root vortex. We see similar aspects captured with regard to the vortices at the tip and root of the blade.

VIII. Conclusions

The benefit of deployable trailing-edge flaps for hovering rotors has been demonstrated via a study based on blade-element methods combined with CFD. Initially, the effect of blade twist on hover performance was quantified using CFD and the results indicated that higher levels of twist provide higher FM at high thrust. Further investigations suggested that increasing blade twist redistributes the loading along the blade, which reduces induced power losses due to high tip loadings. Two optimum flap configurations were then

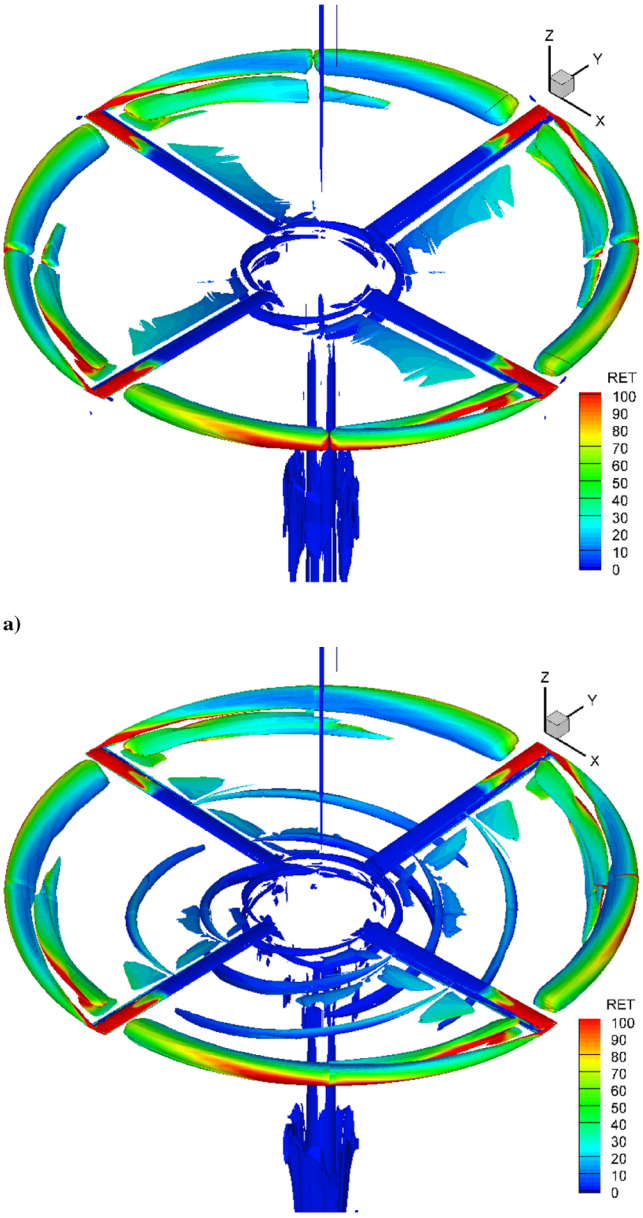

Fig. 7 Isosurfaces of λ_2 colored by the turbulent viscosity ratio for the HIMARCS I rotor in hover: a) −10 deg of twist, b) blended optimum inboard flap; $M_T = 0.627$ and $\lambda_2 = -0.0125$.

selected using the blade-element method. The first was a large inboard flap, which improved the rotor FM by 3–4% at high thrust. Similarly, an outboard flap showed potential to improve the FM by up to 10% at lower thrust.

The inboard slotted flap was implemented on a low-twist rotor and was shown to provide the same levels of performance as a rotor with 6 deg more twist, which included savings in trim angles of approximately 0.5 to 1 deg at high thrust settings. It was indicated by the results that there is a rise in the inboard blade loading when deflecting an inboard flap, with the device having a similar effect as an increase in blade twist and allowing for the reduction in the trim angles. The outboard slotted-flap design, however, did not perform to expectations and failed to offer performance improvements over the baseline rotor. It was concluded that this was due to a combination of strong outboard flap edge vortices generating substantial downwash and a small flap size, hence reducing the overall effectiveness of the flap. The outboard location of the flap would also have the effect of increasing outboard blade loading and increasing induced drag. Interestingly, the optimum outboard configuration was able to achieve savings in trim angles similar to those with the optimum inboard flap, which is itself a benefit.

There are a few areas in which this work could be extended. The effect of turbulence modeling on the predicted blade loads and shed-wake vorticity for validation should be considered, both for improving the code validation and for capturing the flap edge vortices. With respect to the shed wake, the proposition of an inboard or outboard flap would create two potentially serious issues. The first is that an inboard flap on a 4-bladed helicopter will produce 8 inboard vortices that can interact with the fuselage and potentially increase vibration. Similarly, any unsteady loading due to the tip vortex may be altered by the implementation of an outboard flap, which will create two strong flap edge vortices and possibly exacerbate the tip-vortex strength. Finally, considerations for deployment of inboard flaps in forward flight could also be made with respect to retreating blade dynamic stall.

Acknowledgments

The Ph.D. studies of the first author are supported by Westland Helicopters Limited and the University of Glasgow.

References

[1] Friedmann, P. P., and Shanthakumaran, P., "Optimum Design of Rotor Blades for Vibration Reduction in Forward Flight," *Journal of the American Helicopter Society*, Vol. 29, Oct. 1984, pp. 70–80.

[2] Hassan, A. A., and Charles, B. D., "Airfoil Design for Helicopter Rotor Blades-A Three-Dimensional Approach," *Journal of Aircraft*, Vol. 34, Mar.–Apr. 1997, pp. 197–205.

[3] Ganguli, R., and Chopra, I., "Aeroelastic Optimization of an Advanced Geometry Helicopter Rotor," *Journal of the American Helicopter Society*, Vol. 41, Jan. 1996, pp. 18–28.

[4] Datta, A., Sitaraman, J., Chopra, I., and Baeder, J. D., "CFD/CSD Prediction of Rotor Vibratory Loads in High-Speed Flight," *Journal of Aircraft*, Vol. 43, Nov.–Dec. 2006, pp. 1698–1709. doi:10.2514/1.18915

[5] Caradonna, F. X, and Tung. C., "A Review of Current Finite Difference Rotor Flow Methods," *42nd Annual Forum*, AHS International, Alexandria, VA, June 1986, pp. 967–983.

[6] Le Pape, A., and Beaumier, P., "Numerical Optimization of Helicopter Rotor Aerodynamic Performance in Hover," *Aerospace Science and Technology*, Vol. 9, Mar. 2005, pp. 191–201. doi:10.1016/j.ast.2004.09.004

[7] Keys, C., Tarzanin, F., and McHugh, F., "Effect of Twist on Helicopter Performance and Vibratory Loads," 13th European Rotorcraft Forum, Confederation of European Aerospace Societies Paper 2-7, Sept. 1987.

[8] Noonan, K. W., Yeagar, W. T., Singleton, J. D., Wilbur, M. L., and Mirick, P. H., "Wind Tunnel Evaluation of a Helicopter Main-Rotor Blade with Slotted Airfoils at the Tips," NASA Langley Research Center, Rept. NASA-TP- 2001-211260, Hampton, VA, Dec. 2001.

[9] Wachspress, D. A., and Quackenbush, T. R., "BVI Noise Mitigation Via Steady Flap Deflection—An Analysis-Led Test Program," *4th Decennial Specialist's Conference on Aeromechanics* [CD-ROM], AHS International, Alexandria, VA, Jan. 2004.

[10] Gagliardi, A., Beedy, J., Steijl, R., Barakos, G., and Badcock, K. J., "Analysis of Flapped Rotors Using CFD and Indicial Methods," *61st Annual Forum* [CD-ROM], AHS International, Alexandria, VA, June 2005.

[11] Gagliardi, A., and Barakos, G., "Improving Hover Performance of Low-Twist Rotors Using Trailing-Edge Flaps—A Computational Study," *32nd European Rotorcraft Forum* [CD-ROM], Confederation of European Aerospace Societies, Sept. 2006.

[12] Noboru, K., Kondo, N., Saito, S., Akasaka, T., and Tanabe, Y., "An Experimental Study of on Blade Active Tab for Helicopter Noise Reduction," *30th European Rotorcraft Forum* [CD-ROM], Confederation of European Aerospace Societies, Sept. 2004.

[13] Leishman, J. G., *Principles of Helicopter Aerodynamics*, Cambridge Univ. Press, Cambridge, England, U.K., 2002.

[14] Beddoes, T. S., "Practical Computation of Unsteady Lift," *Vertica*, Vol. 8, No. 1, 1984, pp. 55–71.

[15] Leishman, J. G., and Beddoes, T. S., "A Semi-Empirical Model for Dynamic Stall," *Journal of the American Helicopter Society*, Vol. 34, July 1989, pp. 3–17.

[16] Beedy, J., Barakos, G. N., Badcock, K. J., and Richards, B. E., "Using CFD to Improve the WHL Rotor Load Aerodynamic Model," *29th*

European Rotorcraft Forum, Confederation of European Aerospace Societies, Sept. 2004.

[17] Badcock, K. J., Richards, B. E., and Woodgate, M. A., "Elements of Computational Fluid Dynamics on Block Structured Grids Using Implicit Solvers," *Progress in Aerospace Sciences*, Vol. 36, July–Aug. 2000, pp. 351–392.
doi:10.1016/S0376-0421(00)00005-1

[18] Steijl, R., Barakos, G., and Badcock, K., "A Framework for CFD Analysis of Rotors in Hover and Forward Flight," *International Journal for Numerical Methods in Fluids*, Vol. 51, Jan. 2006, pp. 819–847.
doi:10.1002/fld.1086

[19] Spentzos, A., Barakos, G. N., Badcock, K. J., Richards, B. E., Wernert, P., Schreck, S., and Raffel, M., "Investigation of Three-Dimensional Dynamic Stall Using Computational Fluid Dynamics," *AIAA Journal*, Vol. 43, May 2005, pp. 1023–1033.
doi:10.2514/1.8830

[20] Morvant, R., Barakos, G. N., Badcock, K., and Richards, B. E., "Airfoil-Vortex Interaction Using the Compressible Vorticity Confinement Method," *AIAA Journal*, Vol. 43, No. 1, Jan. 2005, pp. 63–75.
doi:10.2514/1.5177

[21] Osher, S., and Chakravarthy, S., "Upwind Schemes and Boundary Conditions with Applications to Euler Equations in General Geometries," *Journal of Computational Physics*, Vol. 50, No. 3, 1983, pp. 447–481.
doi:10.1016/0021-9991(83)90106-7

[22] Roe, P. L., "Approximate Riemann Solver, Parameters Vectors and Difference Schemes," *Journal of Computational Physics*, Vol. 43, No. 2, Oct. 1981, pp. 357–372.
doi:10.1016/0021-9991(81)90128-5

[23] Wilcox, D. C., "Reassessment of the Scale-Determining Equation for Advanced Turbulence Models," *AIAA Journal*, Vol. 26, Nov. 1988, pp. 1299–1310.
doi:10.2514/3.10041

[24] Rogers, S. E., Menter, F., Durbin, P. A., and Mansour, N. N., *A Comparison of Turbulence Models in Computing Multi Element Airfoil Flows*, AIAA Paper 94-0291 Jan. 1994.

[25] Rumsey, C. L., Gatski, T. B., Ying, S. X., and Bertelrud, A., "Prediction of High-Lift Flows Using Turbulent Closure Models," 15th Applied Aerodynamics Conference, AIAA Paper 97-31809, June 1997.

[26] Straub, F. K., "A Feasibility Study of Using Smart Materials for Rotor Control," *Smart Materials and Structures*, Vol. 5, No. 1, 1996, pp. 1–10.
doi:10.1088/0964-1726/5/1/002

[27] Straub, F. K., Ngo, H. T., Anand, V., and Domzalski, D. B., "Development of a Piezoelectric Actuator for Trailing Edge Flap Control of Full-Scale Rotor Blades," *Smart Materials and Structures*, Vol. 10, No. 1, 2001, pp. 25–34.
doi:10.1088/0964-1726/10/1/303

[28] Shin, S., Cesnik, C. E. S., and Hall, S. R., "Closed-Loop Control Test of the NASA/ARMY/MIT Active Twist Rotor for Vibration Reduction," *59th Annual Forum* [CD-ROM], AHS International, Alexandria, VA, May 2003.

[29] Sekula, M. K., Wilbur, M. L., and Yeager, W. T., "Aerodynamic Design Study of an Advanced Active Twist Rotor," *4th Decennial Specialist's Conference on Aeromechanics* [CD-ROM], AHS International, Alexandria, VA, Jan. 2004.

[30] Lemnios, A. Z., and Howes, H. E., "Wind Tunnel Investigation of the Controllable Twist Rotor Performance and Dynamic Behavior," U.S. Army Air Mobility Research and Development Lab., Rept. USA-AMRDL-TR-77-10, Moffett Field, CA, June 1997.